

A Computational Model of a Single-Photon Avalanche Diode Sensor for Transient Imaging

Quercus Hernandez Diego Gutierrez Adrian Jarabo

Universidad de Zaragoza, I3A

Abstract

Single-Photon Avalanche Diodes (SPAD) are affordable photodetectors, capable to collect extremely fast low-energy events, due to their single-photon sensibility. This makes them very suitable for time-of-flight-based range imaging systems, allowing to reduce costs and power requirements, without sacrificing much temporal resolution. In this work we describe a computational model to simulate the behaviour of SPAD sensors, aiming to provide a realistic camera model for time-resolved light transport simulation, with applications on prototyping new reconstructions techniques based on SPAD time-of-flight data. Our model accounts for the major effects of the sensor on the incoming signal. We compare our model against real-world measurements, and apply it to a variety of scenarios, including complex multiply-scattered light transport.

Keywords: Single-photon avalanche diode (SPAD) sensor, Imaging, Photon counting,

Concepts: •Computing methodologies → Sensor modelling;

1 Introduction

Transient imaging has recently emerged, enabling a wide range of applications for computer vision and scene understanding [Jarabo et al. 2017]. Disambiguating light transport in the temporal domain has allowed capturing light in motion [Velten et al. 2013], non-line-of-sight imaging [Velten et al. 2012] or reflectance acquisition [Naik et al. 2011]. However, the used imaging technology is in general too expensive, difficult to operate and time-consuming to be used in the wild.

Photon counting technology, such as single-photon avalanche diodes (SPAD), is a promising technology to address some of these limitations. These detectors are able to detect ultrafast signals, in the order of picosecond resolution, with very high sensitivity, by producing an avalanche current reaction when activated by a photon. They have been demonstrated useful in several fields such as basic quantum mechanics [Rarity and Tapster 1990; Shih and Alley 1988], measurements of fluorescent decays and luminescence in physics, chemistry, biology and material science [Li and Davis 1993; Soper et al. 1993], or single molecule detection [Matem 1983; Andreoni and Cubeddu 1984]. More recently, they have been applied in the particular context of transient imaging, to determine photons time of flight in actively illuminated setups [Garipey et al. 2015]. This has allowed to capture non-line-of-sight objects [Buttafava et al. 2015] with significantly cheaper capturing systems than the previous work [Velten et al. 2012], reducing both the intensity of the scene illumination and the capture times, and in general the complexity and sensitivity of the system.

However, SPADs have a number of negative effects which lead to signal deterioration, such as the time jitter or afterpulsing. Figure 1 shows an example of the temporal response of a SPAD for an impulse signal. In this work we develop a computational model for SPADs, including all relevant effects on the time-resolved signal incoming the sensor, aiming to provide a predictive physically-

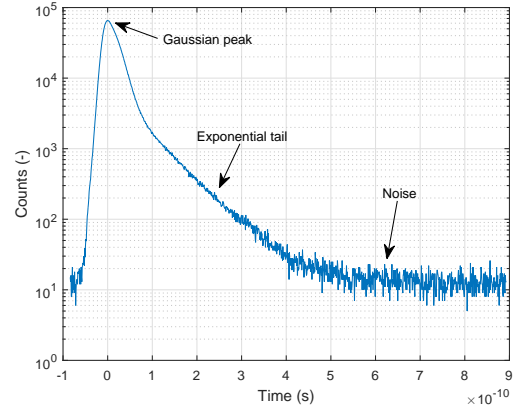


Figure 1: Measured temporal impulse response of a 20 μm CMOS SPAD with excess voltage of $V_e = 20$ V. The curve shows two of the main characteristics of SPAD sensors, including the Gaussian plus exponential shape of the time jitter, as well as the effect of internal and background noise. A filtered normalized version of the curve is used as a data-driven pdf for modelling time jitter in our probabilistic model.

plausible sensor model for transient light transport simulations. This is very important for developing new SPAD-based reconstruction methods, as well as prototyping and assessing the limits of these reconstruction methods before building actual real-world tests. Our model accounts for effects such as the detection efficiency, time jitter, sensor's quenching, internal thermal noise, afterpulsing and pixel's crosstalk. We demonstrate the accuracy of our model comparing against real-world captured data, and apply it on top of complex light transport simulations [Jarabo et al. 2014] showing multiple diffuse interreflections.

2 Related Work

Here we focus on works computationally modeling the behavior of SPADs. We refer to other sources for details on SPADs [Charbon 2007; Kirmani et al. 2014] and transient imaging in general [Jarabo et al. 2017]. The first work focusing on the simulation of SPAD detectors [Zappa et al. 2000] models the electronics of an active quenched circuit. Later, Dalla et al. [2007] describes a circuit model with passive quenching which can be implemented in computer aided software. It can predict precisely the electronic behavior of the avalanche current ignition, quenching and recovery process, although it is restricted to passive quenching. Years later, Mita et al. [2008] and Zappa et al. [2009] presented more complete electronic models including both active and passive quenching. However, these models focus on predicting the low-level electronics of the sensors, neglecting the counting process and the photon source so they cannot be used as camera models for simulation.

Repich et al. [2009] implement a SPAD model for simulating time-resolved fluorescence decay measurements in a fluorophore solu-

tion using Monte Carlo simulation. The target of the paper is to show how imperfections of the sensor affect the results of the measurements. They model the main characteristics of the SPAD detector such as afterpulse, time jitter, dark counts and dead time. However, the dead time is naively implemented as a post-process of the total counts, which might result in rejecting a pulse but not its correlated afterpulse.

Guilinnati et al. [2011] present a physically-based model of SPAD detectors that can accurately reproduce its temporal behavior. Both the photon detector probability and time jitter are fully modeled, but other effects such as afterpulse or quenching are not taken into account. The main goal of the paper is to understand the limitations of the current sensors and discuss some device modifications in order to overcome them.

Finally, Kazma et al. [Kazma et al. 2015] develop a temporal model of the photon arrival time in a SPAD detector. The light source is modelled as a monochromatic laser pulse following a Poissonian distribution. The dead time is applied to the sum of dark counts and source photons, followed by the afterpulsing probability as a post-process. The main drawback of Kazma's method is that it does not take into account the hold-off time of the avalanches generated by the afterpulses. Moreover, it does not model the time jitter of the sensor due to the low temporal resolution of the simulations (milliseconds).

As opposed to these works, our model predicts all temporal and spatial effects of the SPAD on the incoming light signal, including detection efficiency, time jitter, quenching, internal thermal and external noise, afterpulsing and pixel's crosstalk.

3 A Computational SPAD Model

A SPAD detector consists of a reversed biased p-n junction (diode) above its breakdown voltage (V_B), generating a high electric field. The sensor is in a semi-stable state, in which a single photon is able to start an avalanche through the electrons inside the semiconductor layers, generating a measurable electric current. Once the avalanche is triggered, the sensor needs to be quenched and restored to the original voltage so it can detect the next photon. The interval between quenching and restoration is the sensors hold-off time t_o , in which the diode cannot detect other incoming photons. Special phenomena must be taken into account due to external and internal noise or material flaws [Renker 2006; Zappa et al. 2007].

The presented model is defined as a probabilistic model, that simulates most processes occurring in a SPAD as photons arrive. As such, it is defined as a set of probability density functions (pdf), that are sampled in run time. Given the effect each photon on the following ones (due to e.g. SPAD's dead time after quenching), we cannot model the photon arrival as independent stochastic processes, but as a Markovian process. In the following, we describe the different effects of a SPAD, together with their associated pdfs. Later, we explain how these effects are combined into our probabilistic SPAD computational model.

3.1 Photon detection efficiency

In order to be detected, a photon must be absorbed and then trigger the avalanche process. The probability of triggering the avalanche is modelled by the photon-detection efficiency E , defined as the ratio between the number of incoming photons and the number of output pulses as

$$E(\lambda, V_e) = \eta(\lambda) \cdot P_T(V_e), \quad (1)$$

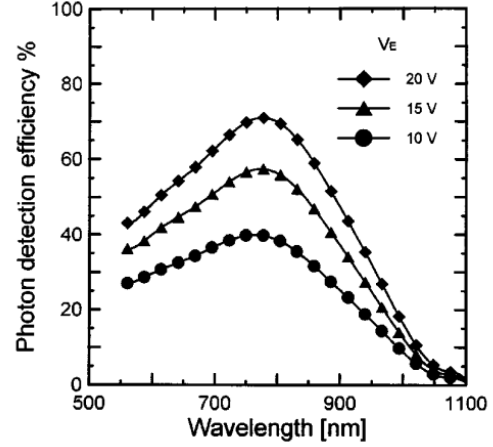


Figure 2: Photon detection efficiency $E(\lambda, V_e)$ as a function of wavelengths for different excess voltage bias. Image from [Cova et al. 1996].

where η is the SPAD absorption efficiency, and $P_T(V_e)$ is the avalanche trigger probability [Savuskan et al. 2013]. The absorption efficiency $\eta(\lambda)$ is related to the physical configuration of the sensor and its material properties, and varies depending on the wavelength λ of the incident radiation. It is given by

$$\eta(\lambda) = (1 - R) \exp(\alpha(\lambda)D) (1 - \exp(\alpha(\lambda)W)) \quad (2)$$

where $\alpha(\lambda)$ is the silicon absorption coefficient, W the depletion region thickness, D the junction depth and R the power reflection coefficient for and air/silicon interface [Zappa et al. 2007].

On the other hand, the avalanche trigger probability $P_T(V_e)$ is a function of the excess voltage of the diode $V_e = V - V_{BD}$, and it is given by

$$P_T(V_e) = P_e(V_e) + P_h(V_e) - P_e(V_e)P_h(V_e), \quad (3)$$

where $P_e(V_e)$ and $P_h(V_e)$ are the probability that an electron and hole respectively will produce an avalanche at x [McIntyre 1973]. These probabilities are proportional to V_e , and can be calculated by using a set of differential equations (see [McIntyre 1973] for the full formulation). However, for low excess voltage the avalanche probability P_T can be approximated using a semi-empirical formula [Dautet et al. 1993; Ghioni et al. 1996]

$$P_T(V_e) \approx 1 - \exp(-V_e/V_c), \quad (4)$$

where V_e is the excess voltage and V_c is the characteristic voltage.

Figure 2 shows different photon detection efficiency curves as a function of wavelength for different excess voltages. In our experiments we set both the excess voltage and wavelength, which allows us to use a fixed efficiency E .

3.2 Time jitter

As photons hit the sensor, their arrival time is captured within an error interval due to the electronics of the SPAD. This error is termed *time jitter*, and is defined as the difference between the real photon arrival time and when it is recorded. This is a very important parameter as it defines the temporal maximum resolution of the sensor (i.e. in particular its point spread function). In general, time jitter t_j is modeled as a characteristic curve obtained with a time-correlated single-photon counting (TCSP) device [O'Connor 2012].

This curve has two well-defined parts (see Figure 1): a Gaussian peak followed by an slower exponential tail as

$$t_j \sim G(\mu, \sigma) + \text{Exp}(\tau). \quad (5)$$

The Gaussian term G is usually defined by the full-width at half-maximum (FWHM) of the curve H_m , which can be directly transformed to the standard deviation using

$$\sigma = \frac{H_m}{2\sqrt{2\ln(2)}}, \quad (6)$$

while the mean value μ is the time when most photons reach the sensor (the maximum count value of the curve). The time constant τ of the exponential distribution is computed following

$$\tau = \frac{W_n^2}{\pi D_e}, \quad (7)$$

where W_n is the thickness of quasi-neutral p region and D_e is the diffusion coefficient of electrons [Lacaita et al. 1989].

Time jitter has been analytically implemented using an exponentially modified Gaussian distribution [Jeansonne and Foley 1991] or by linear blending between both independent distributions [Zhang et al. 2009]. However, since we have access to actual measurements of the sensor, we choose for a data driven approach where t_j is implemented as a tabulated pdf. In order to create a pdf, we filter out the noise, and tabulate and normalize the curve.

3.3 Quenching & Hold-off Time

Once an avalanche is triggered, then the SPAD cannot detect photons. To restore the diode to operating levels, the avalanche must be quenched by lowering the bias below breakdown voltage. This process can be done passively or actively [Tisa et al. 2007b]. Passive circuits are simpler to implement physically, they are prone to errors, imposing a lower temporal resolution and thus reducing their applicability. Here we focus on active quenching circuits.

Active quenching relies on a sophisticated electronic circuit which forces quenching and resets transition in much shorter times. This is achieved by triggering a fast comparator and driving an inverse voltage to the diode in order to force the avalanche to extinct. This makes the system much faster and reliable as the hold-off time t_o is constant in every avalanche process and can be easily adjusted. This hold-off time t_o imposes the non-independence between photon arrival events, transforming our probabilistic model on a Markovian one where the result of each event is dependent on previous states in the chain.

3.4 Internal noise

Due to their high-sensitivity SPADs suffer from errors in form of sensor internal noise, that might trigger incorrect photon counts and therefore degrade the signal. This noise is visible as three effects mainly: dark counts, afterpulsing and crosstalk between neighbor pixels.

3.4.1 Dark counts

Dark counts are thermally generated carriers that can trigger an avalanche process even when the device is operating in dark conditions, resulting in a false count. The probability of dark counts P_{dc} is directly related to the thermal (temperature) and electrical (excess bias voltage) energy of the system, following an exponential relationship [Tisa et al. 2007a], as shown in Figure 3.

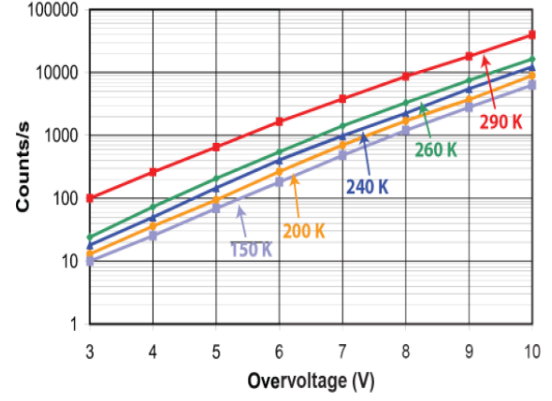


Figure 3: Exponential behavior of dark counts as a function of the excess bias voltage and the temperature. Figure from [Tisa et al. 2007a].

Dark counts are discrete events in a fixed interval of time, well described as a Poisson distribution with mean value the so-called dark count rate R_{dc} :

$$P_{dc} \sim \text{Pois}(k) = \frac{R_{dc}^k \exp(-R_{dc})}{k!}. \quad (8)$$

3.4.2 Afterpulsing

Another source of internal noise, which generates false photon counts, is afterpulsing. It is produced when previous carriers get trapped in the depletion layer, and are later released triggering an additional avalanche with a considerable delay. Afterpulse is modeled as the probability of an avalanche triggering another avalanche after the hold-off time (t_o). The afterpulsing probability P_{ap} is a function of time following an hyperbolic sinc function multiplied by a decreasing exponential function [Horoshko et al. 2014] (see Figure 4). Since in our implementation we fix the hold-off time t_o we use a fixed afterpulse probability P_{ap} for simplicity.

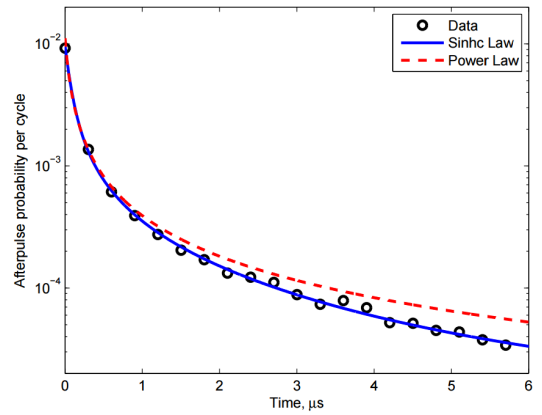


Figure 4: Afterpulse probability P_{ap} as a function of the hold-off time t_o . Source: [Horoshko et al. 2014].

3.4.3 Crosstalk

In applications where 1D or 2D SPAD arrays are required, the electrical isolation of each pixel is crucial to avoid avalanche interfer-

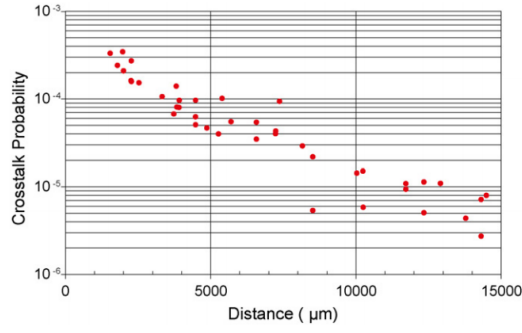


Figure 5: Measured crosstalk probability as a function of the pixel distance in 50 μm SPAD sensors. Source: [Zappa et al. 2007].

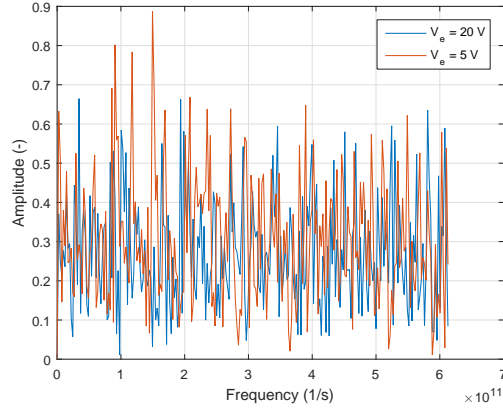


Figure 6: Fourier spectrum of the noise signals of a 20 μm CMOS SPAD with excess voltages of 5 V and 20 V.

ence between adjacent pixels. This optical coupling or crosstalk can be significantly reduced with a correct pixel layout and highly doped isolations diffusions among pixels [Zappa et al. 2007; Rech et al. 2008]. However, even with a correct device design, a crosstalk probability P_{ct} still exists. This crosstalk probability is dependent on the pixel's distance, as shown in Figure 5. While crosstalk noise is rather low, we include it by probabilistic triggering an avalanche on neighbor pixels when a photon arrives to the sensor, based on $P_{ct}(d)$, with d the distance between pixels.

3.5 External noise

Finally, in addition to the internal noise, SPADs are also sensitive to external noise due to ambient light and tunneling effects. This noise is visible in the tail at Figure 1, and it is independent on the SPAD's excess voltage. We analyze the frequency spectrum of the noise in two different noise signals from a 20 μm CMOS SPAD sensor (with voltages at 5 V and 20 V, respectively), and found no dominant frequency (Figure 6). Given the white-noise spectrum and discrete characteristics of the counting process, we model this noise as a Poissonian noise. In our experiments, we set the noise distribution mean P_e to $5 \cdot 10^{11}$ counts/s, calculated from the experimental data in Figure 1.

3.6 Implementation

We implement our probabilistic model as a Matlab function taking as input a list of photons time of arrival, as well as their position

in the case of multiple-pixel sensors. Algorithm 1 describes our model. For computational reasons, both the dark counts and the background noise are added at the end of the simulation, assuming that the probability of triggering afterpulse or crosstalk effects, as well as the effect of the hold-off time of noisy counts, are neglectable.

Data: Ideal input photon arrival time (t_{in}), Simulation time (t_{end})

Result: Histogram of SPAD counts

```

initialization;
for all measurements do
    initialize afterpulse time ( $t_{ap}$ );
    for all input photons do
        if detected ( $E$ ) and not in hold-off time ( $t_{in} > t_{ap}$ ) then
             $t = t_{in} + t_j$ ;
            sum  $t$  to histogram;
             $t_{ap} = t + t_o$ ;
            while  $t_{ap} < t_{end}$  do
                if afterpulse ( $P_{ap}$ ) then
                    sum  $t_{ap}$  to histogram;
                     $t_{ap} = t_{ap} + t_o$ ;
                end
            end
            if crosstalk ( $P_{ct}$ ) then
                sum crosstalk to histogram;
            end
            go back to next input photon;
        else
            go back to next input photon;
        end
    end
end
sum dark counts ( $P_{dc}$ ) to histogram;
sum background noise ( $P_e$ ) to histogram;

```

Algorithm 1: Pseudo-code of our probabilistic SPAD model, transforming the ideal time of arrival of photons into the sensor's response.

4 Results

We evaluate our model under three different scenarios: a time-correlated single-photon counting (TCSP) process, a multiple impulse response, and a more complex temporal response including diffuse interreflections from simulations [Jarabo et al. 2014].

4.1 TCSP simulation

Figure 7 compares our model with respect to captured data for an impulse TCSP process. The captured data comes from measurements of a 20 μm diameter CMOS SPAD sensor with 7 V excess voltage. Two different device bias conditions are considered: a first one optimized for low jitter, i.e. narrow FWHM, and a second one optimized for fast tail. The simulation parameters are shown in Table 1. Our method is able to accurately matching both the temporal response and the internal and external noise of the sensor.

4.2 Multiple impulse simulation

We evaluate our method with two impulse responses arriving the sensor at times 0.6 and 1.2 ns. Given that the dead time of the SPAD is larger than the time resolution, several measurements must be done in order to capture the arrival of several photons with enough

Parameter	Value
Dark count rate	3000 counts/s
Photon detection probability	30 %
Afterpulse probability	1 %
Dead time	10 ns
Background noise	14.7 counts/ps
Time jitter FWHM	26 ps - 36 ps
Time jitter tail	156 ps - 75 ps
Measurements	$3.57 \cdot 10^6$

Table 1: Parameters of our SPAD model used in our simulations.

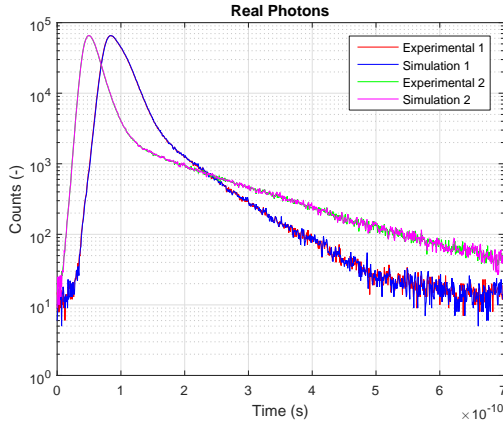


Figure 7: Time-correlated single-photon counting (TCSP) simulations of two different conditions in a SPAD detectors, one with narrow FWHM and other with a longer exponential tail. Our model accurately matches both the time jitter temporal PSF, as well as the signal noise.

precision. Figure 8 shows the SPAD simulation as a histogram of $5 \cdot 10^4$ measurements.

As expected, the first impulse response has slightly more detections than the second one due to the photon detection probability and the hold-off time (with perfect photon detection the second impulse would not be captured). The dark count rate is neglectable at this time scales, as opposed to the background noise. Finally, it can be seen the characteristic Gaussian peak and exponential tail of the sensor’s temporal PSF due to the time jitter.

4.3 Full transport simulation

We additionally evaluate our SPAD model against a more complex light transport response, featuring direct illumination, as well as multiple diffuse interreflections. We use data obtained from time-resolved light transport simulation [Jarabo et al. 2014]. To simulate the sensor response we use the spatio-temporal response output by the transient renderer as a pdf of the incoming photons.

Figure 9 shows an steady-state render of the scene used, while Figure 10 (top) shows an example spatio-temporal response of light transport for a single scanline of the simulation, where the temporal resolution is set to 16.6 ps. Figure 10 (bottom) shows the SPAD response to the ideal incoming radiance on the scanline shown on top, with 10^4 measurements per pixel. As expected, the time jitter of the sensor blurs the temporal response following the PSF defined by the time-jitter curve. This is clearly shown in the first wave front of the streak image. The afterpulsing is also clearly seen as a repetition pattern of the main wavefronts arrival times. It has to be taken

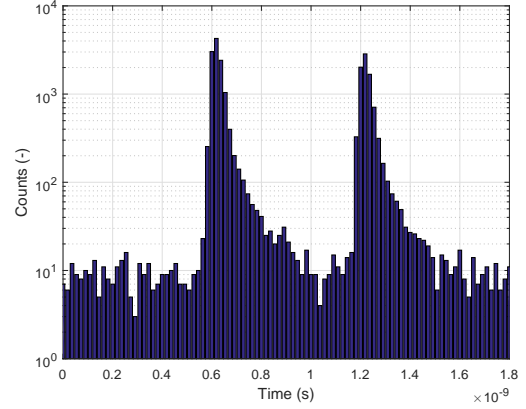


Figure 8: SPAD sensor response for two-impulse incoming signal, with both impulse responses have similar photon counts. Note that the first peak has slightly higher magnitude due to the hold-off time which in a perfect sensor sensitivity would completely mask the second peak of the signal.

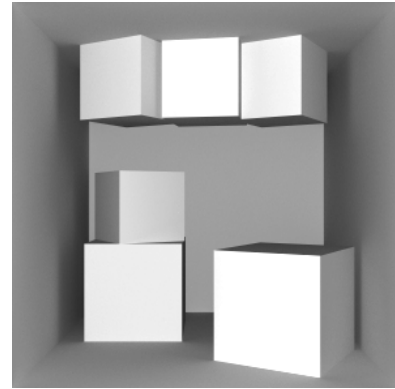


Figure 9: Steady-state render of the scene used to test our model, featuring both impulse response due to direct reflection, as well as multiple diffuse interreflections.

into account that the afterpulse probability was set to $P_{ap} = 1\%$, meaning that only 1% of the photons could potentially trigger a false avalanche. The probability of a n^{th} afterpulse decreases exponentially with probability P_{ap}^n . Note also that the intensity of the diffuse reflections is reduced with respect to the original signal due to hold-off time. Finally, Figure 11 plots the temporal response of a single pixel to directly compare between the incoming ideal signal and the sensor’s response. It shows how the incoming signal exponentially decreases along time due to the sensor’s detection probability and hold-off time, and the added background noise. Note also the afterpulse depicted as a small peak at instant 1.7 ns.

5 Conclusions

In this work we have presented a computational model for single-photon avalanche diodes (SPAD). We posed our model as a probabilistic Markovian model, modeling the sensor response to a set of non-independent photon arrivals. Our work includes most of the effects of SPADs on the output response, including the detection efficiency, time jitter, avalanche quenching, as well as the sensor’s internal and external sources of noise. The goal of our work is to provide an accurate computational sensor model, to be used on top

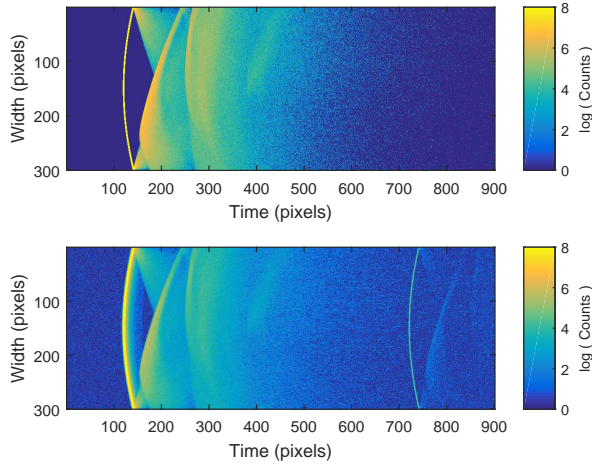


Figure 10: Rendered input spatio-temporal ideal response of the image (top), and the response of the SPAD for that signal. The x-axis represents time (where each pixel represents 16.6 ps), and the y-axis represents an horizontal scanline from Figure 9. Color codes photon counts in logarithmic scale.

of physically-based transient light transport simulations: This is important to use these simulations on the development of new computational techniques for image understanding on transient imaging, where SPAD sensors have emerged as a promising low-cost and highly-efficient imaging technology.

Acknowledgements

We want to thank Alberto Tosi and his team at Politecnico di Milano for providing references on SPADs theory and characterization, as well as measured data from real-world SPADs. This research has been funded by DARPA (project REVEAL), and the Spanish Ministerio de Economía y Competitividad (projects TIN2016-78753-P and TIN2014-61696-EXP).

References

- ANDREONI, A., AND CUBEDDU, R. 1984. Photophysical properties of photofrin ii in different solvents. *Chemical Physics Letters* 108, 2, 141 – 144.
- BUTTAFAVA, M., ZEMAN, J., TOSI, A., ELICEIRI, K., AND VELTEN, A. 2015. Non-line-of-sight imaging using a time-gated single photon avalanche diode. *Opt. Express* 23, 16 (Aug), 20997–21011.
- CHARBON, E. 2007. Will avalanche photodiode arrays ever reach 1 megapixel. In *International Image Sensor Workshop*.
- COVA, S., GHIONI, M., LACAITA, A., SAMORI, C., AND ZAPPA, F. 1996. Avalanche photodiodes and quenching circuits for single-photon detection. *Appl. Opt.* 35, 12 (Apr), 1956–1976.
- DALLA MORA, A., TOSI, A., TISA, S., AND ZAPPA, F. 2007. Single-photon avalanche diode model for circuit simulations. *IEEE Photonics Technology Letters* 19, 23, 1922–1924.
- DAUTET, H., DESCHAMPS, P., DION, B., MACGREGOR, A. D., MACSWEEN, D., MCINTYRE, R. J., TROTTIER, C., AND WEBB, P. P. 1993. Photon counting techniques with silicon avalanche photodiodes. *Applied Optics* 32, 21, 3894–3900.

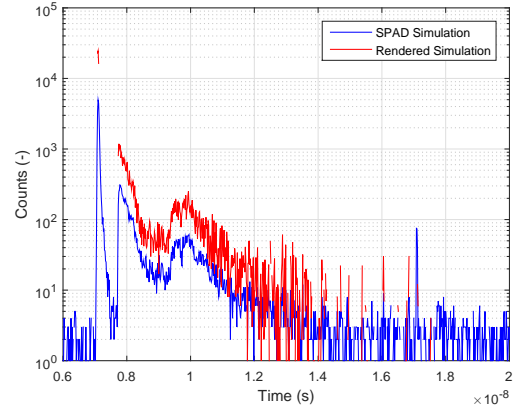


Figure 11: Single-pixel temporal response of the ideal simulated response of the scene at Figure 9 (red), and the response of the SPAD to that input image (blue).

- GARIEPY, G., KRSTAJIĆ, N., HENDERSON, R., LI, C., THOMSON, R. R., BULLER, G. S., HESHMAT, B., RASKAR, R., LEACH, J., AND FACCIO, D. 2015. Single-photon sensitive light-in-flight imaging. *Nature Communications* 6.
- GHIONI, M., COVA, S., ZAPPA, F., AND SAMORI, C. 1996. Compact active quenching circuit for fast photon counting with avalanche photodiodes. *Review of Scientific Instruments* 67, 10, 3440–3448.
- GULINATTI, A., RECH, I., ASSANELLI, M., GHIONI, M., AND COVA, S. 2011. A physically based model for evaluating the photon detection efficiency and the temporal response of spad detectors. *Journal of Modern Optics* 58, 3-4, 210–224.
- HOROSHKO, D., CHIZHEVSKY, V., AND KILIN, S. Y. 2014. Full-response characterization of afterpulsing in single-photon detectors. *arXiv preprint arXiv:1409.6752*.
- JARABO, A., MARCO, J., MUÑOZ, A., BUISAN, R., JAROSZ, W., AND GUTIERREZ, D. 2014. A framework for transient rendering. *ACM Transactions on Graphics (SIGGRAPH Asia 2014)* 33, 6.
- JARABO, A., MASIA, B., MARCO, J., AND GUTIERREZ, D. 2017. Recent advances in transient imaging: A computer graphics and vision perspective. *Visual Informatics* 1, 1.
- JEANSONNE, M. S., AND FOLEY, J. P. 1991. Review of the exponentially modified gaussian (emg) function since 1983. *Journal of chromatographic science* 29, 6, 258–266.
- KAZMA, R., ROSSETTO, O., AND SICARD, G. 2015. High level model of spad based pixel. In *Ph. D. Research in Microelectronics and Electronics (PRIME), 2015 11th Conference on*, IEEE, 125–128.
- KIRMANI, A., VENKATRAMAN, D., SHIN, D., COLAÇO, A., WONG, F. N., SHAPIRO, J. H., AND GOYAL, V. K. 2014. First-photon imaging. *Science* 343, 6166.
- LACAITA, A., GHIONI, M., AND COVA, S. 1989. Double epitaxy improves single-photon avalanche diode performance. *Electronics letters* 25, 13, 841–843.
- LI, L., AND DAVIS, L. M. 1993. Single photon avalanche diode for single molecule detection. *Review of Scientific Instruments* 64, 6, 1524–1529.

- MATEM, F. 1983. A semiconductor detector for measuring ultra-weak fluorescence decays with 70 ps fwhm resolution.
- MCINTYRE, R. J. 1973. On the avalanche initiation probability of avalanche diodes above the breakdown voltage. *IEEE Transactions on Electron Devices* 20, 7, 637–641.
- MITA, R., PALUMBO, G., AND FALLICA, P. G. 2008. Accurate model for single-photon avalanche diodes. *IET circuits, devices & systems* 2, 2, 207–212.
- NAIK, N., ZHAO, S., VELTEN, A., RASKAR, R., AND BALA, K. 2011. Single view reflectance capture using multiplexed scattering and time-of-flight imaging. *ACM Trans. Graph.* 30.
- O’CONNOR, D. 2012. *Time-correlated single photon counting*. Academic Press.
- RARITY, J. G., AND TAPSTER, P. R. 1990. Experimental violation of bell’s inequality based on phase and momentum. *Phys. Rev. Lett.* 64 (May), 2495–2498.
- RECH, I., INGARGIOLA, A., SPINELLI, R., LABANCA, I., MARANGONI, S., GHIONI, M., AND COVA, S. 2008. A new approach to optical crosstalk modeling in single-photon avalanche diodes. *IEEE Photonics Technology Letters* 20, 5, 330–332.
- RENKER, D. 2006. Geiger-mode avalanche photodiodes, history, properties and problems. *Nuclear Instruments and Methods in Physics Research Section A: Accelerators, Spectrometers, Detectors and Associated Equipment* 567, 1, 48–56.
- REPICH, M., STOPPA, D., PANCHERI, L., AND DALLA BETTA, G.-F. 2009. Simulation modelling for the analysis and the optimal design of spad detectors for time-resolved fluorescence measurements. In *SPIE Europe Optics+ Optoelectronics*, International Society for Optics and Photonics, 73550O–73550O.
- SAVUSKAN, V., BROUK, I., JAVITT, M., AND NEMIROVSKY, Y. 2013. An estimation of single photon avalanche diode (spad) photon detection efficiency (pde) nonuniformity. *IEEE Sensors Journal* 13, 5, 1637–1640.
- SHIH, Y. H., AND ALLEY, C. O. 1988. New type of einstein-podolsky-rosen-bohm experiment using pairs of light quanta produced by optical parametric down conversion. *Phys. Rev. Lett.* 61 (Dec), 2921–2924.
- SOPER, S. A., MATTINGLY, Q. L., AND VEGUNTA, P. 1993. Photon burst detection of single near-infrared fluorescent molecules. *Analytical Chemistry* 65, 6, 740–747.
- TISA, S., TOSI, A., AND ZAPPA, F. 2007. Fully-integrated cmos single photon counter. *Opt. Express* 15, 6 (Mar), 2873–2887.
- TISA, S., ZAPPA, F., TOSI, A., AND COVA, S. 2007. Electronics for single photon avalanche diode arrays. *Sensors and Actuators A: Physical* 140, 1, 113–122.
- VELTEN, A., WILLWACHER, T., GUPTA, O., VEERARAGHAVAN, A., BAWENDI, M. G., AND RASKAR, R. 2012. Recovering three-dimensional shape around a corner using ultrafast time-of-flight imaging. *Nature communications* 3, 745.
- VELTEN, A., WU, D., JARABO, A., MASIA, B., BARSİ, C., JOSHI, C., LAWSON, E., BAWENDI, M., GUTIERREZ, D., AND RASKAR, R. 2013. Femto-photography: Capturing and visualizing the propagation of light. *ACM Trans. Graph.* 32, 4.
- ZAPPA, F., GHIONI, M., COVA, S., SAMORI, C., AND GIUDICE, A. C. 2000. An integrated active-quenching circuit for single-photon avalanche diodes. *IEEE Transactions on instrumentation and measurement* 49, 6, 1167–1175.
- ZAPPA, F., TISA, S., TOSI, A., AND COVA, S. 2007. Principles and features of single-photon avalanche diode arrays. *Sensors and Actuators A: Physical* 140, 1, 103–112.
- ZAPPA, F., TOSI, A., DALLA MORA, A., AND TISA, S. 2009. Spice modeling of single photon avalanche diodes. *Sensors and Actuators A: Physical* 153, 2, 197–204.
- ZHANG, D., AMMO, H., RYU, J., SUMI, H., AND NISHIMURA, T. H., 2009. A modeling and evaluation of the random telegraph signal noise on a cmos image sensor in motion pictures.